

SUSTAINABLE SYNTHESIS AND CHARACTERIZATION OF TUNABLE AND MULTIPURPOSE NANOCELLULOSE FROM FRESHWATER AQUATIC WEED AS PHARMACEUTICAL EXCIPIENT

KESHAV S. MOHARIR* , KRISHNAKANT B. BHELKAR , VINITA V. KALE , ABHAY M. ITTADWAR

Department of Pharmaceutics, Gurunanak College of Pharmacy, Nagpur
Email: keshavmoharir@gmail.com

Received: 17 Dec 2022, Revised and Accepted: 03 Jan 2023

ABSTRACT

Objective: The main objective of this work was to understand the basic properties of crystalline nanocellulose (CNC) that can be useful as a novel excipient in pharmaceutical formulations. This covers the isolation and preparation of nanocellulose followed by characterization.

Methods: Cellulose was isolated from aquatic weed by autoclaving and bleaching. Cellulose to CNC conversion involved gluconic acid treatments at different concentrations (40%, 50% and 60%) followed by centrifugation and neutralization. CNC was further characterized by Differential Scanning Calorimetry (DSC) and Thermo gravimetric Analysis (TGA), Field Emission Scanning Electron Microscopy (FE-SEM) and Atomic Force Microscopy (AFM) for surface morphology, elemental analysis by Energy Dispersive Spectroscopy (EDS), Fourier Transform Infrared Spectroscopy (FTIR), crystallinity index by X-Ray Diffraction (XRD), and optical microscopy.

Results: Acid concentration affects the moisture uptake, particle size, and yield of CNC. CNC size ranged from 350 nm to 900 nm with a crystallinity index 80% to 85%. Moisture uptake was $6.38 \pm 0.12\%$ at 33% relative humidity. DSC and TGA established thermal stability over 200 °C. Nanocellulose has shown Angle of repose (28.81°), Carrs index (12.32), zeta potential (33mV) values and heavy metals within pharmacopoeial limits.

Conclusion: CNC from water hyacinth was prepared successfully by sustainable process. CNC physico-chemical characterization revealed the stable nature of CNC, suitable to be used as an excipient in pharmaceutical formulations.

Keywords: Nanocellulose, Excipient, Drug delivery, Characterization, Water hyacinth

© 2023 The Authors. Published by Innovare Academic Sciences Pvt Ltd. This is an open access article under the CC BY license (<https://creativecommons.org/licenses/by/4.0/>)
DOI: <https://dx.doi.org/10.22159/ijap.2023v15i2.47100>. Journal homepage: <https://innovareacademics.in/journals/index.php/ijap>

INTRODUCTION

The progress in drug delivery systems in last couple of decades has seen giant leap from conceptualization to actual utility in terms of excipient and adjuvant research. Be it synthetic drug, biologicals, biosimilars, and natural extractives; pharmaceutical excipients have the lion's share to make the drug exhibit its pharmacological actions at the correct time, correct location, in correct manner and with minimum unwanted effects. The quest for newer excipients and drug carriers is not only restricted to novel drug delivery systems but also, they are in demand for conventional pharmaceutical formulations [1]. The correct answer to the question why we at all need novel pharmaceutical excipients lies in the fact that they impart stability to the API (active pharmaceutical ingredients), improve dissolution rate, help to deliver the drug at target location, improve taste, enhance aesthetic value, prolong the drug release, maintain immunogenicity in vaccines, and impart ease of handling via their tunable physico-chemical properties. These excipients truly exert 'behind the scenes' role, with latest example as the incorporation of lipid membranes in mRNA vaccine for COVID-19 developed by Moderna and Pfizer/BioNTech as an effective means of career system [2].

In this context, novel excipients are being continuously searched and developed with an eye on nanomaterials owing to their several advantages such as high surface area, high drug loading capacity, target specific drug delivery, predictable drug release kinetics, and possible customizable approaches in their applications. In recent years, the focus has shifted more towards bionanomaterials, that too of biodegradable nature. While several factors are involved in selection of suitable bionanomaterials in drug delivery systems, current trend highlights exploration of natural polymers and their composite structures. Some of these include chitosan, sodium alginate, pectin, cellulose, gelatin, natural gums, dextran, agarose, proteins, peptides, clays like bentonite, etc. These natural nanoparticulate drug carriers can be broadly classified as organic, inorganic and metal oxides. Among all of these biodegradable, biocompatible, inexpensive bionanocarriers, cellulose is most abundant on the earth having noteworthy inherent mechanical, chemical, structural and biological properties [3]. In addition,

nanocellulose properties are tunable, it is recyclable, promising sustainable alternative to current biodegradable and natural nanoparticles in several aspects of drug delivery systems. Being "green material", it has been the mainstay area of extensive research for last few years in the field of drug delivery and biomedical applications [4]. Based on the sources and method to obtain it, nanocellulose can be classified as Crystalline Nanocellulose (CNC), Crystalline Nanofibers (CNF) and Bacterial Nanocellulose (BNC) [5]. The application of each of them changes with perspective of their preparation method and ensuing physico-chemical properties [6].

Numerous sources to obtain nanocellulose have been reported such as sugarcane bagasse, kenaf, cotton, sugar beet, wheat straw, bamboo, tunicates, algae, eucalyptus, garlic skin, to quote a few among many that span among plant, animal, bacterial and civil waste origin [7]. Several excellent reviews are available that throw light on sources, extraction and isolation processes of nanocellulose. For conversion of cellulose to nanocellulose, hydrophobic and amorphous lignin as well as hemicellulose regions must be broken by overcoming the phenolic group and xylan-glucomannan bonds respectively present in them [8]. The harsh conditions are required stepwise that include alkali treatment such as 4% to 10% NaOH (w/v) for removal of amorphous hemicellulose for varying time and temperature conditions reported by several researchers. Similarly, removal of lignin needs strong acidic treatment primarily reported as sulphuric acid, phosphoric acid, hydrochloric acid at 30% to 65% concentration level running for several minutes to few hours at ambient temperatures 40 °C to 120 °C. Sizeable works also mention use of bleaching agents H₂O₂ and acidified sodium chlorite as means of delignification [9]. In a process to obtain CNF from raw cellulose, 2,2,6,6-Tetramethylpiperidine-1-oxyl radical (TEMPO), a strong oxidizing agent is used as catalyst often rated as hazardous environment material [10]. Taking into consideration adverse environmental impact of these harsh chemicals and excess quantity of water required at each step of neutralization, modern methods such as use of ultrasonication, ionic liquids and deep eutectic solvents (DES). However, each of these modern methods pose limitation/s; either has higher cost element, being environmentally toxic or require higher input of energy in various ways [10].

With overall discussion, this work proposes a sustainable method to synthesize nanocellulose with minimum harm to the environment utilizing gluconic acid that will support UN sustainable development goals number 13, 14 and 15 (<https://sdgs.un.org/goals>). Water hyacinth (*Eichhornia crassipes* Mart.) was selected as the source of cellulose. Water hyacinth is an invasive aquatic species that is detrimental to aquatic health by blocking sunlight, restricts water flow and multiplies rapidly (<https://www.invasivespeciesinfo.gov/aquatic/plants/water-hyacinth>). Notwithstanding with this, water hyacinth has tremendous applications in multiple fields, and the drug delivery system is no exception [11]. Literature is abundant with the characterization of nanocellulose; nevertheless, fundamental and derived properties of nanocellulose intended for drug delivery systems are lacking. In this study, we present an evaluation of nanocellulose derived from water hyacinth that includes particle size by dynamic light scattering (DLS) and size distribution, thermal properties by DT-TGA and DSC, FT-IR, test of heavy metals, surface morphology by FE-SEM and atomic force microscopy, crystallinity by XRD, flow properties, compressibility index, proximate analysis (% moisture, ash value,) and optical study of nanoparticles. These studies will be discussed specifically with perspectives and requirements of pharmaceutical excipients and drug carriers.

MATERIALS AND METHODS

Raw material collection and crystalline nanocellulose (CNC) preparation

Biomass collection

The common water hyacinth *Eichhornia crassipes* was collected from a nearby pond and water lagoons in Nagpur district, Maharashtra State, India (geographical co-ordinates 21° 09'42.2"N 79° 06'46.7"E). Collected water hyacinth was authenticated as *Eichhornia crassipes* at Department of Botany, Rashtrasant Tukadoji Maharaj Nagpur University, Nagpur, India (Herbarium Sheet no. 10228). Stem part was selected for further studies, followed by a cleaning and drying process under shed. Sodium hypochlorite, sodium hydroxide, gluconic acid were of AR grade purchased from HiMedia, Mumbai, India.

Extraction of biomass

Weighed quantity of dried and finely grinded # 60 mesh sieved WH stem powder was soaked in mixture of NaOCl (3%v/v) and NaOH (3%w/v) in the ratio 1:10 for 60 min. The mass-to-liquid ratio was 1: 5 expressed by weight. This mass was then subjected to autoclaving at 121 °C at 15 psi pressure for 30 min. Post-autoclaving cycle, filtration of the pulp with Whatman filter paper number 41 was carried out for maximum yield. After filtration, a copious volume of distilled water was added for neutralization, confirmed by calibrated digital pH meter (Hanna Instruments Inc, Model HI2202). The yield was calculated on weight basis.

Nanocellulose preparation

Crystalline nanocellulose was prepared by acid hydrolysis with gluconic acid. Gluconic acid is an organic acid, one of the very few mild organic acids with nontoxic, noncorrosive, biodegradable, Generally Regarded as Safe (GRAS accepted) and nonvolatile nature [12]. Filtered pulp of the previous step was used on dry basis for nanocellulose synthesis. In brief, 40 g dried pulp was added to 400 ml gluconic acid in the ratio 1:10 on a weight basis (40%, 50% and 60% w/v solution as received from the supplier). The resultant slurry was subjected to intense homogenization at 10,000 rpm for 5 min held in between 55 °C to 58 °C using homogenizer (Kinematica AG Polytron PT 3100 D Switzerland, 1200, 50Hz). This chemical-mechanical treatment was arrested by adding equal volume chilled distilled water. The process was repeated for 3 passes; dispersion was allowed to reach room temperature, followed by centrifugation for 5 min at 5000 rpm. To maximize the yield, centrifugation was carried out thrice. The supernatant CNC dispersion was neutralized to pH 7 by keeping it in dialysis membrane, this being kept in distilled water bath for dialysis for 4 d. Since gluconic acid exhibited dark brown color, bleaching was carried out for decolorization with 2% sodium hypochlorite (NaOCl) by weight at 50 °C for 30 min in CNC to NaOCl ratio of 1:5 (20 g CNC in 100 ml NaOCl). The CNC dispersion was

further neutralized using dialysis membrane for 4 d and filtered subsequently. The yield was calculated on a dry weight basis. The obtained CNC was further subjected to evaluation tests.

Characterization of CNC

Proximate analysis

World Health Organization recommends standardization of herbal drugs and natural excipients used in pharmaceutical formulations, often backed by Pharmacopoeial standards of relevant countries [13].

Moisture absorption studies

The moisture uptake by CNC was carried out on wet weight basis at 25 °C for two extremes of humidity maintained at 33 % RH and 86% RH respectively by saturated solutions (200 ml) of MgCl₂.6H₂O and ZnSO₄.7H₂O in separate desiccators [14]. The sample size was 5 g, spread evenly as thin layer in a tared petri plate kept in a desiccator and following equation was used.

$$\text{Moisture absorption} = [(W_m - W_0)/W_0] \times 100 \dots (1)$$

Where W_0 is the initial weight after drying the sample at 105 °C for 2 h in hot air oven and W_m is the weight at equilibrium after moisture absorption. The process was repeated thrice, the absorption was measured for 48 h [15].

Determination of total ash value

Ash value was determined by the method described in Indian Pharmacopoeia 2018. Briefly, 2 g CNC sample was weighed and transferred to a pre-heated silica crucible, again weighed and transferred to muffle furnace. Sample was heated at 600 °C for 2 h. Crucible was removed from the furnace, allowed to reach room temperature in a desiccator and weighed again. Following equation was used to calculate total ash value

$$\text{Total ash content} = [(a-b)/c] \times 100 \dots (2)$$

Where: a = sample weight and petri dish before drying (g)

b = sample weight and petri dish after drying (g)

c = sample weight before drying (g)

Acid insoluble ash

Ash collected from the previous total ash content method was weighed and boiled in 2M HCl for 5 min followed by filtration using ashless filter paper (Whatman filter paper no. 42). After washing with hot water sample was ignited in muffle furnace at 600 °C for 2 h, cooled in a desiccator and weighed [16].

$$\text{Acid insoluble ash} = \frac{\text{weight of acid insoluble ash}}{\text{Weight of sample}} \times 100 \dots (3)$$

CNC powder flow properties characterization

In 50 ml glass measuring cylinder, 10 g CNC sample was introduced for bulk and tapped density estimation. Untapped volume yielded bulk density while tapped density was obtained after tapped volume from equations (4) and (5), respectively. The tapping on hard surface till constant volume in ml was determined in accordance with United States Pharmacopoeia 2018 (USP 41-NF 36). In continuation, these results were used to further calculate Hausners ratio and Carr's compressibility index employing equation (6) and (7) respectively. The process was replicated thrice.

$$\text{Bulk density} = \frac{\text{Mass}}{\text{Untapped volume}} \dots (4)$$

$$\text{Tapped Density} = \frac{\text{Mass}}{\text{Tapped volume}} \dots (5)$$

$$\text{Hausners ratio} = \frac{\text{Tapped density}}{\text{Bulk density}} \dots (6)$$

$$\text{Carr's compressibility index} = \frac{\text{Tapped density} - \text{Bulk density}}{\text{Tapped density}} \times 100 \dots (7)$$

Pharmaceutical powders need to be free-flowing while handling and formulations processes. Accordingly, static angle of repose was determined to ascertain flow pattern of CNC powder. A glass funnel mimicking hopper was fixed on stand with its lower end held above 5 cm from the hard, flat surface. Weighed 10 g sample was passed through the funnel of nominal internal diameter 10 mm at 25 °C. This conventional method employed formula $\tan^{-1}(h/r)$. In addition, dynamic angle of repose was also determined by using transparent glass barrel of length 10 cm and internal diameter 4 cm. Random angle powder made while rotating was measured during rotations and average was used in calculations [17].

Compressibility studies

The elastic or plastic behavior of powders in limited space by volume reduction under pressure can be predicted by Kawakita plot and equation. Although not full proof, it gives rough estimation of compressibility of samples under test. Method described by Patil *et al.* was used with modification [18]. Equation (8) describes the terms and parameters of Kawakita plot.

$$\frac{P}{C} = \frac{P}{a} + \frac{1}{ab} \dots\dots (8)$$

Where, C is reduction in volume on compression under pressure P , constants a and b are obtained when P/C is plotted against P . The analysis was intended to check efficacy of CNC in direct compression. With 1% magnesium stearate as lubricant, CNC was directly compressed at compression force 3,4,5 and 6 kN to form 10 mm, 450 mg tablet.

Particle size measurement by Dynamic Light Scattering DLS

Hydrodynamic diameter-based particle size of CNC was determined by dynamic light scattering (Litesizer™ 500, Anton Paar, Austria). Sample (approximately 0.01% w/v) was prepared by sonication of CNC dispersion to avoid clumps or agglomerates.

Surface morphology characterization

Field emission scanning electron microscopy (FE-SEM) of CNC

The surface morphology of CNC obtained at different concentrations of gluconic acid treatment was evaluated by FE-SEM under vacuum at an accelerating voltage range 20kV (JEOL JSM 6380A). Dimension, shape and structural properties were observed at high resolution.

Atomic force microscopy (AFM) of CNC

The atomic force microscopy was operated with tapping mode of silicon tip to estimate crystalline surface at ambient temperature. Surface topology was observed in 3D view with respect to changing gluconic acid concentration. AFM was executed using a Bruker MultiMode 8 version microscope with a ScanAsyst-Air probe and FASTSCAN-B controller. The tip with low spring constant of 1.8 N/m, resonant frequency 450 kHz, a silicon cantilever tip diameter of 5 nm in tapping was employed.

Aqueous dispersion stability

In several types of pharmaceutical formulations, nanoparticles may face brief or longer contact time with solvents or different fluids. Irrespective of solubility behavior, the stability of CNC in water can be estimated for brief period of time by knowing zeta potential of the samples. Diluted 0.01% w/v CNC dispersion in distilled water was analyzed for zeta potential at 25 °C (Litesizer™ 500, Anton Paar, Austria).

Elemental analysis by energy dispersive X-ray spectroscopy (EDS)

The elemental composition of CNC was evaluated by EDS technique. EDS helps to detect elements present, mainly semi qualitative and semi quantitative data to know contaminants presence, both of exo- and endogenous nature [19]. The elements present emitting X-rays were determined with corresponding energy level in 1-20 KeV range. The sample was prepared as a thin layer and with coating of conductive Pt layer.

X-ray diffraction (XRD) and crystallinity index (CI)

The crystallinity of the CNC was analyzed by powder X-ray diffraction study (Bruker-AXS D8 Advance). The study was performed using Cu radiation generated at 25 mA intensity and 35 kV voltage at wavelength 1.5406 Å. The XRD pattern was obtained between 3° to 90° (2θ). From the same diffractogram, crystallinity index was calculated by peak height method reported by Segal *et al.* [20]. The empirical formula for CI calculation is as follows

$$\text{Crystallinity index} = \frac{I_{002} - I_m}{I_{002}} \times 100 \dots\dots (9)$$

Where I_{002} height of heights peak

I_m height of lowest peak

FT-IR analysis

Uniform size CNC samples were dried for 2 h at 60 °C prior to analysis. Samples were homogeneously mixed with KBr. Shimadzu IRAffinity 1800 was used for FT-IR spectra with 64 scans in the range 400 cm^{-1} to 4000 cm^{-1} . For each sample, three spectra were recorded. CNC synthesized by different gluconic acid concentration CNC40, CNC50 and CNC60 were compared with microcrystalline cellulose.

Optical microscopy studies

Dried powder samples were observed under optical microscopy in dark field mode at 10X and 40X resolution attached with high resolution camera (Motic Image Plus 2.0 China). The purpose of this study was to understand the structural arrangement of CNC crystals that could not be observed through FE-SEM. Optical microscope with high-resolution video camera was used to capture the images. For this, dispersion of CNC in distilled water (0.01% w/v) was prepared at neutral pH diluted sufficiently suitable for observation.

Thermal analysis

Differential Scanning Calorimetry (DSC) and Thermogravimetric Analysis (TGA)

Differential scanning calorimeter of CNC sample was carried out (TA Instruments SDT Q600 V20.9 Build 20) and thermograms were obtained with the temperature increment at the rate 10 °C/minute to 400 °C. To maintain inert environment, nitrogen purging was ensured throughout analysis. The sample weight loss was evaluated from the TGA curve of weight loss (%) versus temperature (°C). DSC study was held to study the chronological influence of changing temperature on CNC characteristic crystallization, glass transition temperature (T_g) and fusion [21].

RESULTS AND DISCUSSION

The native cellulose possesses crystalline as well as amorphous regions. To get cellulose enriched fraction, removal of lignin and hemicellulose is necessary which is mainly achieved by acid hydrolysis/alkali treatments, although other methods exist. This step costs upto 40% of total cost of CNC production. To reduce this cost, we combined NaOH (3%w/v) alkalinized bleach sodium hypochlorite (3% v/v) for synergistic effect. Suspended raw cellulose in these chemicals when subjected to autoclaving, steam releasing step burst opened the hydrophobic regions. With further stirring for 2 h at 55 °C this separated hemicellulose and lignin from crystalline cellulose. Upon washing and till neutral through dialysis membrane, yield was 66.88% by weight. Next, homogenization at 10,000 rpm for 30 min in presence of gluconic acid transversely breaks the tightly held cellulosic bonds that are not cleaved during chemico-mechanical autoclaving step. Gluconate ions replace H⁺ probably at 5th carbon position (since gluconic acid is a weak acid, it is less likely to attack stronger β1-4 glycosidic bonds that attach successive cellulose molecules). The subsequent steps include washing, neutralization by dialysis, centrifugation and then sonication, spray drying or freeze drying to get final product.

The eco-friendly, sustainable method to obtain nanocellulose with gluconic acid is possible due to source of cellulose; water hyacinth

which is non-hard wood and low in lignin, hemicellulose content as compared to hard wood, tough sources [22]. The cellulose extraction from soft wood permits milder conditions in delignification and

isolation process, thus it was possible to attempt use of mild organic acid like gluconic acid [23]. The reaction taking place in gluconic acid induced cellulose hydrolysis can be summarized in fig. 1.

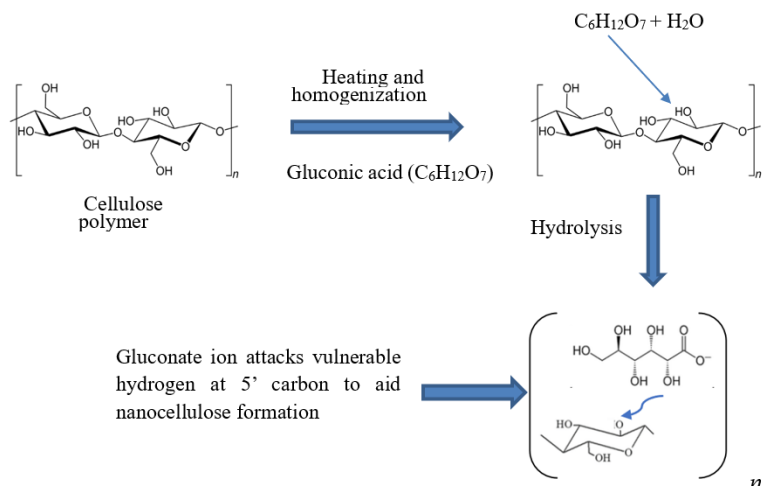
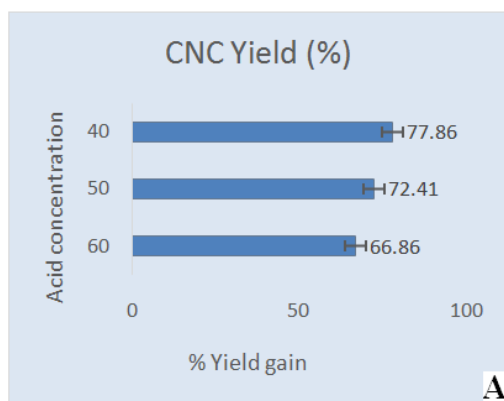


Fig. 1: Hydrolysis process of cellulose by gluconic acid

Fig. 2 shows collectively raw material and different physical forms of CNC. At concentration up to 0.75% (w/v), CNC forms hazy dispersion which gradually becomes viscous and ultimately forms gel above 2% concentration. Yield of CNC is higher at lower acid

concentration, 77.86 ± 2.32 (% by weight), 72.41 ± 1.56 (% by weigh) and 66.86 ± 2.32 (% by weight) for 40%, 50% and 60% gluconic acid concentration. This may be due procedural loss of smaller particle size formed at higher acid concentrations [24].



(n=3)

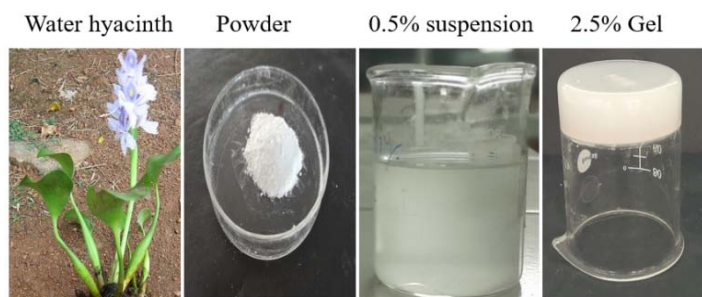


Fig. 2: Yield of CNC (A) and forms of CNC obtained from raw material (B)

Proximate analysis

The moisture or water absorption rate in pharmaceutical excipients helps to understand what will be the temporal water diffusion quantity in final formulation. Since many drugs are water sensitive,

this study helps to understand the compatibility and selection criteria of drug-nanocellulose in the formulation. At 33% RH, the total moisture absorbed after 48 h was $6.89 \pm 0.74\%$ while at 86% RH, moisture absorption was $9.21 \pm 0.78\%$, which is beyond the permissible limit. That means, below the median relative humidity

of the range selected (around 60% RH) if CNC is used in solid dosage forms, stability can be ensured under proper storage conditions [25]. The moisture uptake by CNC is a phenomenon that depends on charge of ions, in this case gluconate, the Coulombic forces and weak Van der Waals forces. The higher acid concentration leads to smaller surface area, thus more chances of water uptake [26]. Moisture

absorption of CNC is higher in comparison with MCC, might be due to more hydrophilic gluconate presence on the CNC surface. However, this property may help in bond formation after compression-relaxation phenomenon during tableting. It is to be remembered that this is the moisture absorption rate over a time period, not total moisture content.

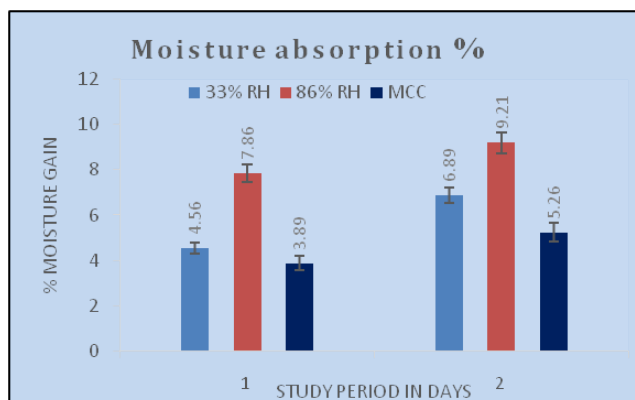


Fig. 3: Moisture absorption of CNC compared with MCC (n=3)

Since the plant origin excipients may be having different levels of extraneous matter owing to their geographical and regional differences, total ash value and acid insoluble ash of pure drug is to be compared with the test sample. Although there are no set criteria for acceptance limit of these values of CNC, 5.87±0.54% total ash and acid insoluble ash of inorganic matter 1±0.14% was found to be within pharmacopoeial standards for herbal powders.

Powder flow characteristics

Several unit processes in pharmaceutical industries such as mixing, granulation, tableting, filling, in common require prior knowledge of powder flow behaviour, micromeritics that include information about density, and angle of repose. Although these values are very dependent on several factors such as method, quantity, particle size distribution, a rough idea helps to understand necessary changes to

be made in given excipient to make it suitable for use in formulations. CNC when subjected to static angle of repose using a fixed funnel, observed values for 40%, 50%, and 60% gluconic acid CNC treated were 32.45°±0.12, 30.96°±0.08 and 28.81°±0.02 respectively. For same treatment regimens, dynamic angle of repose using transparent rotating drum had respective values 31.38°±0.11, 30.11°±0.02 and 27.47°±0.12 after triplicate studies (n=3). The increased acid concentration was linked to smaller particle size and better flow and hence lower angle of repose [27]. In addition, bulk and tapped density have significant place in pharmaceutical formulations. Packing behaviour of CNC is a function of particle size, size distribution which in turn depends upon acid concentration, temperature and duration of cellulose treatment. At 40% acid concentration, crystallinity is lower and higher amorphous region as compared to 60% acid level [28].

Table 1: Flow properties of CNC

Gluconic acid concentration % w/v	Characteristic properties				
	Bulk density (g/ml) (mean±SD)	Tapped density (g/ml) (mean±SD)	Angle of repose (mean±SD)	Carr's index (mean±SD)	Hausners ratio (mean±SD)
40%	0.33±0.012	0.42±0.001	32.45°±0.12	16.22±0.12	1.27±0.10
50%	0.28±0.026	0.40±0.009	30.96°±0.08	12.68±1.06	1.40±0.12
60%	0.27±0.011	0.39±0.021	28.81°±0.02	12.32±0.23	1.03±0.18
MCC (Sancel®)	0.28±0.033	0.38±0.012	23.35±0.08	10.85±0.24	1.22±0.15

(n=3)

The Carr's compressibility index and Hausners ratio findings indicate that higher gluconic acid concentration makes cellulose more crystalline, thus making it difficult for compression. At an amorphous-crystalline moderate level, CNC has acceptable density properties with ability to pack in void spaces that is otherwise difficult with fag ends of crystalline and amorphous powders. The comparison of commercial grade MCC and CNC has slight differences in the density and Carr's index. The better flow behaviour of MCC reflected by Carr's index and Hausners ratio can be attributed to monodisperse particle size and cohesiveness of CNC particles. Smaller CNC particles at higher humidity tend to come closure due to prevailing van der Waals forces of attractions and thus at closer distance, exhibit poor flow. However, this issue can be overcome by spray drying of CNC. The above results are consistent with previous studies by Kolakovic *et al.* [29]. As seen from table 1, MCC values have an edge over CNC, the combination as a co-processed excipient of CNC-MCC can make a still better choice in future.

Compressibility studies

Kawakita plot is rough expression of the ability of powder or granules to flow cohesively and get compressed under different compression pressures. From equation (8), P/c indicates ratio of compression pressure to degree of volume reduction after a cumulatively increasing number of taps. We see that there is near to linearity in volume reduction of CNC after taps corresponding to the increased pressure. That means compression behaviour is fairly predictable that can be adjusted to desired characteristics as required. The plot in fig. 4 indicates all types of CNC under study and MCC undergo non elastic volume reduction on tapping even after standing of 24 h. However, the data obtained does not give details of the compaction pattern difference between direct compression vs wet granulation with binder. In general, blend of crystals with different particle sizes gives better compressibility as compared to monodispersed crystals, this also holds true for CNC [30].

Particle size analysis and aqueous dispersion stability by dynamic light scattering

Hydrodynamic diameter-based particle size and size distribution was determined by dynamic light scattering (Litesizer™ 500, Anton Paar, Austria). The samples were ultrasonicated to remove any air bubbles that can hamper actual results. The average hydrodynamic diameter of diluted CNC was observed to decrease with increasing acid

concentration, at 40% gluconic acid concentration, average particle size was 917 ± 18 nm while for 60% gluconic acid level, average particle size was 379 ± 18 nm as shown in fig. 5. But at the same time, it was noted that stability, as reflected by zeta potential, is better at higher acid concentration (60%, 50%, and 40%) treatment corresponding to 33.6 ± 1.1 mV, 26.4 ± 0.3 mV and -12.8 ± 0.6 mV. The negatively charged gluconate ions give net anionic charge to the CNC, resulting in repulsion and hence more stability at higher acid concentrations [31].

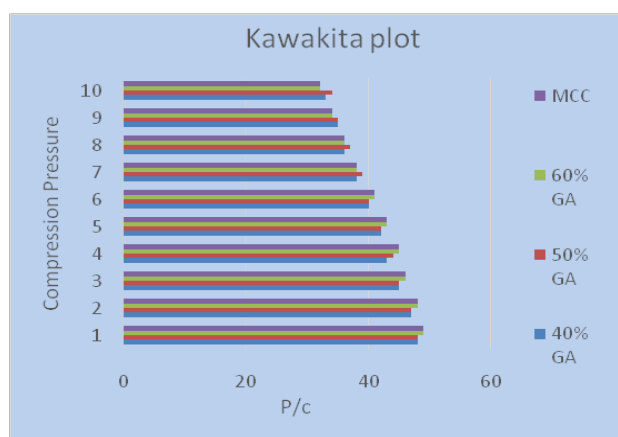


Fig. 4: Effect of apparent compression pressure on volume reduction of CNC obtained from different acid concentrations (n=3)

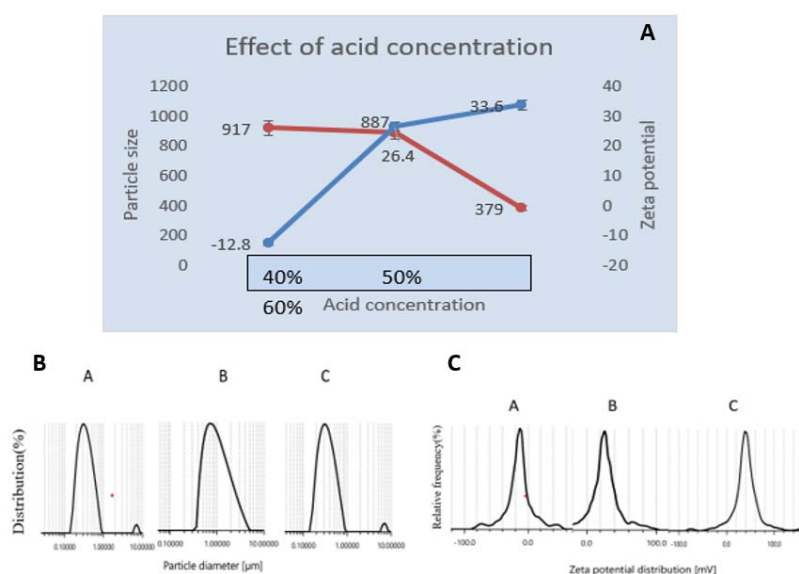


Fig. 5: Average particle diameter of CNC and zeta potential depicting effects of acid concentration (A), particle size distribution (B), and zeta potential at different concentrations (C) (n=3)

As pharmaceutical excipients in different capacities, CNC prepared from various acid ratios can contribute to aqueous dispersion as clear from zeta potential [32].

Surface morphology and topography

The applications and utility of pharmaceutical excipients changes with change in the final dosage forms, so do the steps involved. Tablets, capsules, emulsions, suspensions, solutions, powders, and suppositories are the most common formulations till date. In each of them, surface properties and structure play important role in unit processes like milling, mixing, dissolution, crystallization, drying, compression, flow uniformity, density, packing, and cohesiveness. Thus, prepared CNC were evaluated for surface morphology and topography.

FE-SEM reveal that at lower acid concentrations crystals of CNC has aspect ratio up to 20 while as the acid treatment becomes longer and

higher side, crystals take the shape of fine needle and with an aspect ratio up to 40. This aspect ratio of CNC can be finely controlled and tuned to manage *in vivo* pharmacokinetics of the drug by controlling drug dissolution from the formulations [33]. Not only this, the aspect ratio of nanoparticles is also known to influence cellular uptake in targeted drug delivery systems [34]. The fig. 6(A) shows rod-shaped CNC crystals dominating among all while another FE-SEM image shows high aspect ratio CNC crystals. The orderly crystal structure can have a profound effect on solubility, melting and thermal activity when formulated with drugs in a dosage form.

FE-SEM only shows 2D images of objects with length x width dimensions. AFM gives an idea about 'surface feel' of nanoparticles that helps to understand grain size, surface roughness, nano-mechanical frictional forces, and surface energy. These studies are extremely useful in preformulation and formulation studies before

the development of novel drug delivery systems [35](Lamprecht *et al.*, 2014). Represented here are the B1 and B3 surface topography by tapping mode of 40% and 60% acid-treated CNC while B2 and B4 show corresponding phase images in 10 μm scan size. The surface in 40% acid-treated CNC (B3 and B4) appear comparatively smooth as compared to 60% acid-treated CNC (B1 and B2), largely due to difference in the crystal size, shape and lattice structure. Later show particle size around 45 nm while B3 and B4 show around 290 nm. DLS has limitations in size determination of hydrodynamic diameter while AFM shows better

size due to dry nature. B1 and B2 also show ‘peak and valley’ pattern showing highly crystalline structure. Topographically, the difference in colours like dark and white indicate differences in roughness, particle size and rough/smooth structure. In short, at higher acid concentrations, CNC structure become more rough, adhesion properties, and crystalline suggesting changed physical properties that may influence pharmaceutical formulations [37]. Further, 3D-AFM images can help understand structure-force relationship at molecular levels and at close distances that can influence the pharmacokinetics of the drug [38, 39].

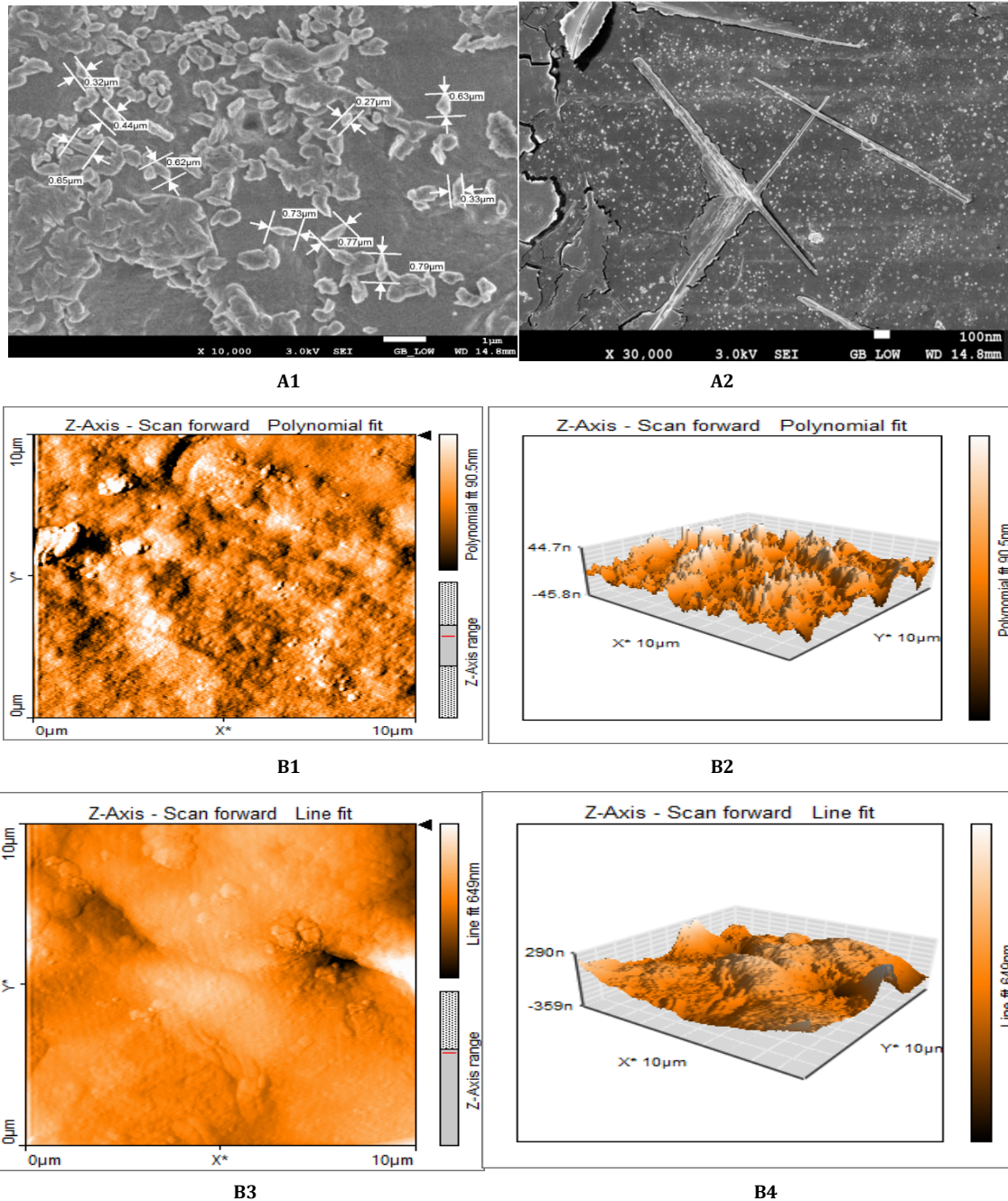


Fig. 6: Field emission scanning electron microscopy (FE-SEM) of CNC (A1 and A2) and atomic force microscopy (AFM) of CNC (B1, B2, B3 and B4). 3D-AFM images describe and correlates surface roughness with tapping mode images

Elemental analysis by energy dispersive X-ray spectroscopy (EDS)

Energy dispersive x-ray spectroscopy (EDS) assisted with FESEM was used to determine elemental composition of CNC. In fig. 8, the EDS spectrum shows the distinct peaks corresponding to carbon,

oxygen with platinum and phosphorus. The appearance position of these peaks corresponds to binding energies. Corresponding to their binding energies. The amount of carbon (52.6%) and oxygen (44.9%) are consistent with existing data [40]. Platinum appears in traces due to platinum sputtering/coating of the sample during sample

preparation to make it conductive. Impurity is observable as phosphorous in small quantities; the source may be attributed to sodium hypochlorite. However, EDS cannot detect hydrogen as it lacks

electrons [41]. The spectrum confirms the absence of any other elements expect those mentioned above, confirming water hyacinth as an alternative source of CNC for proposed pharmaceutical excipients.

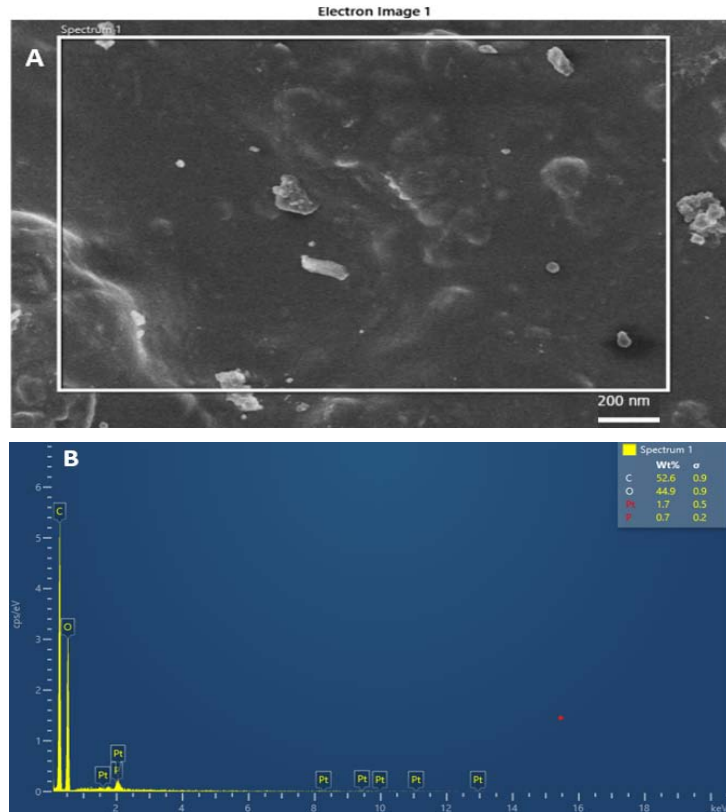


Fig. 7: Electron capture image for elemental analysis (A), and elemental composition of CNC (B) X-ray diffraction (XRD) and crystallinity index (CI)

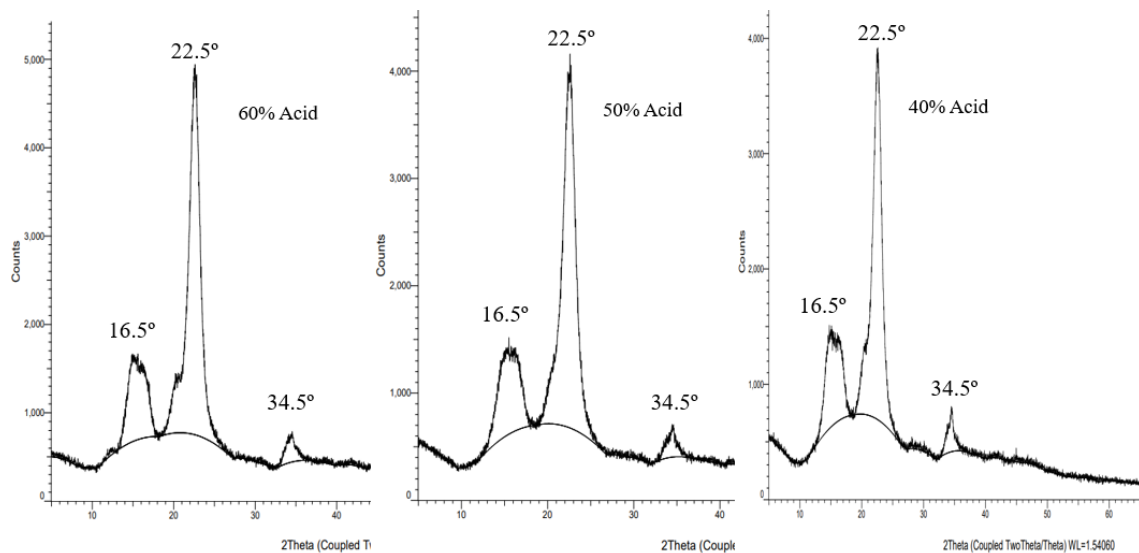


Fig. 8: X-ray diffraction (XRD) patterns of CNC treated with different concentrations of gluconic acid

In XRD studies of CNC, the peaks obtained from 40%, 50% and 60% gluconic acid were almost superimposable. Typical structure of type I cellulose was indicated with sharp peaks at $2\theta = 16.5^\circ$, 22.4° and 34.5° in all the diffractograms [42]. The characteristic highest peak at 22.6° confirms the crystalline structure of CNC as also reflected in AFM surface morphology. With the Segal method of crystallinity

index (CI) determination, it was found that for 40%, 50% and 60% respectively CI was 79.48%, 83.33%, and 85.71%. Although CI was not significantly different, there did exist a difference in flow properties, density and compaction behaviour of three types of CNC under discussion. On the same lines, even slight difference in CI may bring about changes in crystal size, specific surface area, and aspect

ratio that may in turn affect compaction patterns, gel strength, redispersability, disintegration and dissolution of the drug from dosage forms [43]. In short, it can be concluded that higher the acid concentration, removal of amorphous regions from raw cellulose is better with higher CI values.

FT-IR analysis

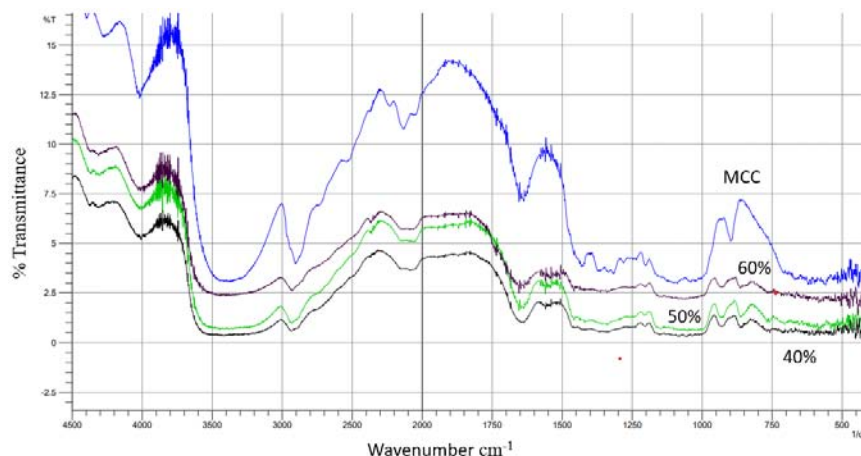


Fig. 9: FT-IR of CNC. Shows four spectra of microcrystalline cellulose (MCC), 40%, 50% and 60% gluconic acid treated cellulose

Fig. 9 shows 4 main peaks observable at 3500-3900 cm^{-1} , 3000-2800 cm^{-1} , 1750-1500 cm^{-1} , and around 100-800 cm^{-1} . The peak in the range 3500-3900 cm^{-1} corresponds to the stretching of hydrogen bonds interactions from-OH group while the C-H stretching is characteristic for the range 2800-3000 cm^{-1} . The most interesting peaks that confirm presence of CNC is range 1000-896 cm^{-1} corresponding to β 1-4 glycosidic linkages of cellulose [45]. A specific, common peak in all

samples around 1650 cm^{-1} corresponds to absorbed water, the low peak intensity correlating with low moisture absorption and low water vapor transmission rate of CNC fibers [46, 47]. As a reference peak of MCC, all the bonds and groups are preserved in the CNC. The peaks at wavelength 1315 cm^{-1} in all samples could be assigned to angular deformation and bending vibrations due to the C-H and C-O groups, corresponding to the aromatic ring specific to polysaccharide [48].

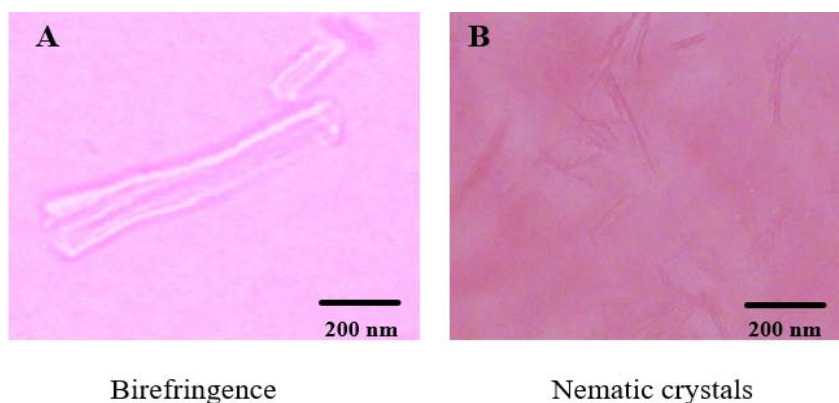


Fig. 10: Optic microscopy studies. Plane polarized light on optical microscope (A) and TEM showing self arranging CNC crystals (B)

Optical microscopy and transmission electron microscopy (TEM) studies

The CNC particles exhibit peculiar features when subjected to polarized light. Amorphous particles do not show interference color while crystals show changes in colour, at least the intensity changes occur at edges and borders of the crystals as appears in fig. 10 (A). TEM of CNC show long crystals of CNC that is in agreement with structures observed by AFM and FE-SEM. The nematic crystal arrangement visible in TEM changes to isotropic as pH of CNC dispersion becomes more acidic. This can be attributed to the deposition of more gluconate anions that repel each other and prevent aggregation of CNC crystals [49].

Fig. 10(A) reveals the contours of CNC rod-like crystals with edges having different refractive indices. Furthermore, both images reaffirm the high aspect ratio of CNC. These properties are highly

favorable for pharmaceutical formulations that aid in convenient handling and amenable to unit processes [50].

Thermal analysis Differential Scanning Calorimetry (DSC) and Thermogravimetric Analysis (TGA)

Pharmaceutical excipients are continuously exposed to a variety of surrounding conditions, individually or in the presence of other chemicals in the final formulations. Change in handling temperature with respect to storage environments, processing variations, relative humidity, and the presence or absence of water has a profound effect on the quality and efficacy of final product. Differential Scanning Calorimetry (DSC) and Thermogravimetric Analysis (TGA) studies revealed the behaviour of CNC at ramping temperature (10 $^{\circ}\text{C}/\text{min}$) and its corresponding effect on Tg (glass transition temperature), degradation pattern, and exothermic/ endothermic nature [51].

The TGA Curve of CNC pyrolysis is biphasic, revealing chronological sequence of events. Initially, there is dehydration till 233 °C after which decomposition occurs rapidly. Initial weight loss could be attributed to the evaporation of held water and loss of the number of-OH groups. Weight loss of approximately 7% till 233 °C tells us

thermal stability of CNC that can be perceived as acceptable in pharmaceutical formulations since this temperature is rarely required in routine procedures [48]. Beyond this temperature, there occurred about 53% weight loss of the sample by the formation of charred product.

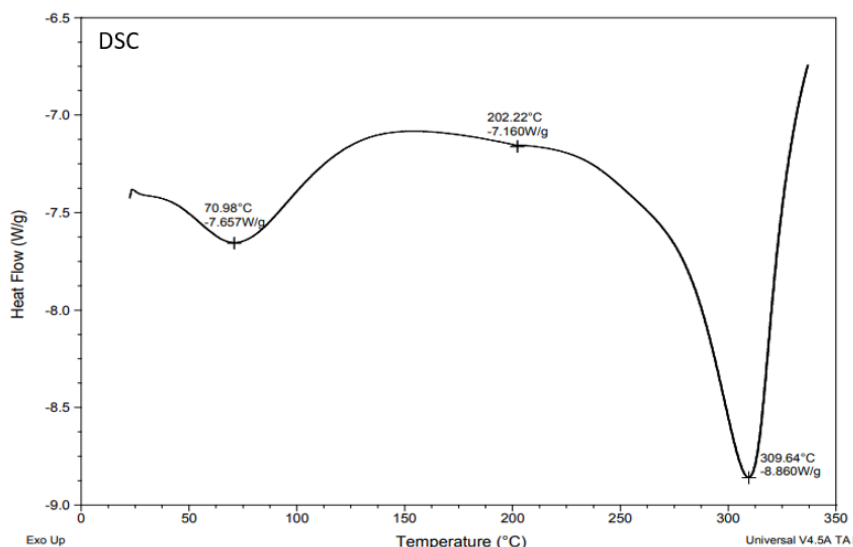


Fig. 11: DSC curve of CNC

The DSC curve of CNC shows glass transition temperature T_g at 71 °C. The T_g value for CNC from water hyacinth being soft wood was found to be lower than that of hardwood sourced CNC. The following exothermic cold crystallization at 202 °C is weak, indicating only small

amorphous region while melting in endothermic melting around 309.64 °C is sharp. This sharp melting curve indicates thermoplastic behaviour of CNC below this temperature that is commonly found suitable and acceptable for pharmaceutical polymers [52, 53].

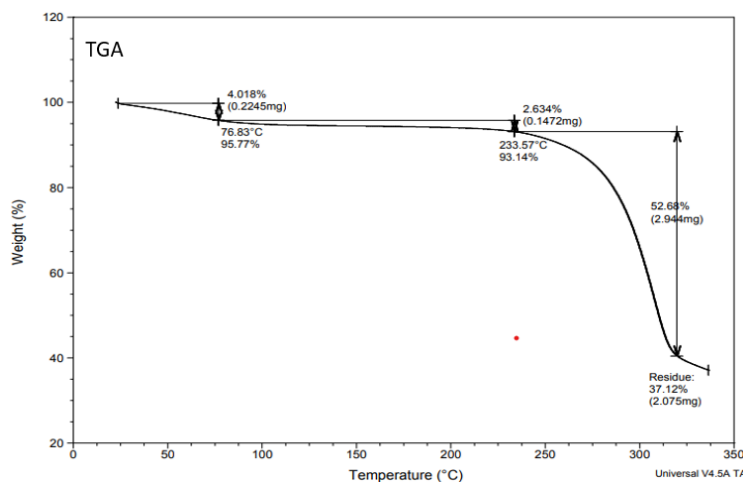


Fig. 12: Thermal analysis Differential Scanning Calorimetry (DSC) and Thermogravimetric Analysis (TGA)

CONCLUSION

This work underlines the evaluation of CNC from natural biomass as a novel excipient for pharmaceutical formulations. CNC nanoparticles were successfully isolated using environment-friendly, biodegradable, non-toxic, GRAS-accepted gluconic acid. The isolated CNC was characterized and critically evaluated for its suitability in pharmaceutical adjuvant that included its water vapor transmission rate, surface topology and morphology, flow properties, crystal structure, thermal properties by DSC and TGA, FE-SEM, elemental analysis by EDS, FTIR, crystallinity index by XRD, and optical microscopy by TEM. The pharmacopoeial standards generally required for the qualification of products such as tablets,

capsules, suspensions, emulsions, powders can be fulfilled by easy management of the physico-chemical properties of CNC obtained from water hyacinth. In addition, CNC can be reinforced with several other polymers to enhance the native CNC properties.

Particle size distribution (300 nm to 900 nm), zeta potential (33mV to -12.6mV), birefringence, gel-forming at high concentration (2.5% by weight and above), high crystallinity (80% to 85%), lower moisture absorption rate (6.38% to 9.21%), minimal impurity in manufacturing process evidenced by FT-IR and EDS are few of the glimpses of water hyacinth derived CNC. Thus, based on these results, CNC from water hyacinth from 'naive' gluconic acid can be produced even on a large scale as a sustainable product for

incorporation into pharmaceutical formulations as a nonactive excipient.

FUNDING

Nil

AUTHORS CONTRIBUTIONS

All the authors have contributed equally.

CONFLICT OF INTERESTS

Declared none

REFERENCES

- Bin LK, Gaurav A, Mandal UK. A review on co-processed excipients: current and future trend of excipient technology. *Int J Pharm Pharm Sci*. 2019 Jan 1;11(1):1. doi: 10.22159/ijpps.2019v11i1.29265.
- Kiran Misra S, Pathak K, Pathak D, Yadav R. Current updates on COVID-19 vaccines. *Asian J Pharm Clin Res*. 2021 Mar 7:17-23. doi: 10.22159/ajpcr.2021.v14i5.41061.
- Vora R, Yamini S. Investigation of critical material attributes of nanocellulose in tablets. *Asian J Pharm Clin Res*. 2019 May 29:256-65.
- Das S, Ghosh B, Sarkar K. Nanocellulose as sustainable biomaterials for drug delivery. *Sens Int*. 2022;3:100135. doi: 10.1016/j.sintl.2021.100135.
- Klemm D, Kramer F, Moritz S, Lindström T, Ankerfors M, Gray D. Nanocelluloses: A new family of nature-based materials. *Angew Chem Int Ed Engl*. 2011 Jun 6;50(24):5438-66. doi: 10.1002/anie.201001273, PMID 21598362.
- Salimi S, Sotudeh Gharebagh R, Zarghami R, Chan SY, Yuen KH. Production of nanocellulose and its applications in drug delivery: A critical review. *ACS Sustainable Chem Eng*. 2019 Oct 7;7(19):15800-27. doi: 10.1021/acssuschemeng.9b02744.
- Kaur P, Sharma N, Munagala M, Rajkhowa R, Aallardyce B, Shastri Y. Nanocellulose: resources, physio-chemical properties, current uses and future applications. *Front Nanotechnol*. 2021;3. doi: 10.3389/fnano.2021.747329. Available from: <https://www.frontiersin.org/articles/10.3389/fnano.2021.747329>.
- Phanthong P, Reubroycharoen P, Hao X, Xu G, Abudula A, Guan G. Nanocellulose: extraction and application. *Carbon Resour Convers*. 2018 Apr;1(1):32-43. doi: 10.1016/j.crcon.2018.05.004.
- Eichhorn SJ, Etale A, Wang J, Berglund LA, Li Y, Cai Y. Current international research into cellulose as a functional nanomaterial for advanced applications. *J Mater Sci*. 2022 Mar 3;57(10):5697-767. doi: 10.1007/s10853-022-06903-8.
- Jonoobi M, Oladi R, Davoudpour Y, Oksman K, Dufresne A, Hamzeh Y. Different preparation methods and properties of nanostructured cellulose from various natural resources and residues: a review. *Cellulose*. 2015;22(2):935-69. doi: 10.1007/s10570-015-0551-0.
- Dufresne A. Nanocellulose processing properties and potential applications. *Curr For Rep*. 2019;5(2):76-89. doi: 10.1007/s40725-019-00088-1.
- Ma Y, Li B, Zhang X, Wang C, Chen W. Production of gluconic acid and its derivatives by microbial fermentation: process improvement based on integrated routes. *Front Bioeng Biotechnol*. 2022 May 16;10:864787. doi: 10.3389/fbioe.2022.864787, PMID 35651548.
- Rose N, Kamta E, Namdeo P, Samal PK. Standardization strategies for herbal drugs-an overview. *Res J Pharm Technol*. 2008;1(4):310-2.
- The control of humidity by saturated salt solutions. Available from: <http://iopscience.iop.org/0950-7671/25/3/305>. [Last accessed on 11 Feb 2023]
- Vilela C, Morais JD, Silva ACQ, Munoz Gil D, Figueiredo FML, Silvestre AJD. Flexible nanocellulose/lignosulfonates ion-conducting separators for polymer electrolyte fuel cells. *Nanomaterials (Basel)*. 2020 Aug 29;10(9):1713. doi: 10.3390/nano10091713, PMID 32872554.
- Liu K. New and improved methods for measuring insoluble acid ash. *Anim Feed Sci Technol*. 2022;288:115282. doi: 10.1016/j.anifeedsci.2022.115282.
- Beakawi Al-Hashemi HM, Baghabra Al-Amoudi OS. A review on the angle of repose of granular materials. *Powder Technol*. 2018;330:397-417. doi: 10.1016/j.powtec.2018.02.003.
- Patil S, Pandit A, Godbole A, Dandekar P, Jain R. Chitosan based co-processed excipient for improved tableting. *Carbohydr Polym Technol Appl*. 2021;2:100071. doi: 10.1016/j.carpta.2021.100071.
- Scimeca M, Bischetti S, Lamsira HK, Bonfiglio R, Bonanno E. Energy dispersive X-ray (EDX) microanalysis: a powerful tool in biomedical research and diagnosis. *Eur J Histochem*. 2018 Mar 15;62(1):2841. doi: 10.4081/ejh.2018.2841, PMID 29569878.
- Segal L, Creely JJ, Martin AE, Conrad CM. An empirical method for estimating the degree of crystallinity of native cellulose using the X-ray diffractometer. *Text Res J*. 1959 Oct 2;29(10):786-94. doi: 10.1177/004051755902901003.
- Gill P, Moghadam TT, Ranjbar B. Differential scanning calorimetry techniques: applications in biology and nanoscience. *J Biomol Tech*. 2010;21(4):167-93. PMID 21119929.
- Owonubi SJ, Agwuncha SC, Malima NM, Shombe GB, Makhatha EM, Revaprasadu N. Non-woody biomass as sources of nanocellulose particles: a review of extraction procedures. *Front Energy Res*. 2021 Apr 8;9. doi: 10.3389/fenrg.2021.608825.
- Syafri E, Sudirman, Mashadi, Yulianti E, Deswita, Asrofi M. Effect of sonication time on the thermal stability, moisture absorption, and biodegradation of water hyacinth (*Eichhornia crassipes*) nanocellulose-filled bengkuang (*Pachyrhizus erosus*) starch biocomposites. *J Mater Res Technol*. 2019 Nov;8(6):6223-31. doi: 10.1016/j.jmrt.2019.10.016.
- Wang J, Xu J, Zhu S, Wu Q, Li J, Gao Y. Preparation of nanocellulose in high yield via chemi-mechanical synergy. *Carbohydr Polym*. 2021;251:117094. doi: 10.1016/j.carbpol.2020.117094, PMID 33142632.
- Blanco D, Antikainen O, Raikonen H, Yliruusi J, Juppo AM. Effect of colloidal silicon dioxide and moisture on powder flow properties: predicting in-process performance using image-based analysis. *Int J Pharm*. 2021;597:120344. doi: 10.1016/j.ijpharm.2021.120344, PMID 33545294.
- Garg M, Apostolopoulou-Kalkavoura V, Linares M, Kaldeus T, Malmstrom E, Bergstrom L. Moisture uptake in nanocellulose: the effects of relative humidity, temperature and degree of crystallinity. *Cellulose*. 2021 Sep 29;28(14):9007-21. doi: 10.1007/s10570-021-04099-9.
- Wang C, Huang H, Jia M, Jin S, Zhao W, Cha R. Formulation and evaluation of nanocrystalline cellulose as a potential disintegrant. *Carbohydr Polym*. 2015 Oct;130:275-9. doi: 10.1016/j.carbpol.2015.05.007, PMID 26076627.
- Sartika D, Syamsu K, Warsiki E, Fahma F. Optimization of sulfuric acid concentration and hydrolysis time on crystallinity of nanocrystalline cellulose: A response surface methodology study. *IOP Conf Ser.: Earth Environ Sci*. 2019 Nov 1;355(1):012109. doi: 10.1088/1755-1315/355/1/012109.
- Kolakovic R, Peltonen L, Laaksonen T, Putkisto K, Laukkanen A, Hirvonen J. Spray-dried cellulose nanofibers as a novel tablet excipient. *AAPS PharmSciTech*. 2011;12(4):1366-73. doi: 10.1208/s12249-011-9705-z, PMID 22005956.
- Trivedi R, Prajapati P. Nanocellulose in the packaging industry. In: *Nanocellulose materials*. Elsevier; 2022. p. 43-66.
- Kumar P, Miller K, Kermanshahi Pour A, Brar SK, Beims RF, Xu CC. Nanocrystalline cellulose derived from spruce wood: influence of process parameters. *Int J Biol Macromol*. 2022 Nov;221:426-34. doi: 10.1016/j.ijbiomac.2022.09.017, PMID 36084872.
- Barbosa AM, Robles E, Ribeiro JS, Lund RG, Carreno NLV, Labidi J. Cellulose nanocrystal membranes as excipients for drug delivery systems. *Materials (Basel)*. 2016 Dec 12;9(12):1002. doi: 10.3390/ma9121002, PMID 28774122.
- Liu Y, Tan J, Thomas A, Ou-Yang D, Muzykantov VR. The shape of things to come: the importance of design in nanotechnology

- for drug delivery. *Ther Deliv.* 2012;3(2):181-94. doi: 10.4155/tde.11.156, PMID 22834196.
34. Parakhonskiy B, Zyuzin v MV, Yashchenok A, Carregal Romero S, Rejman J, Möhwald H. The influence of the size and aspect ratio of anisotropic, porous CaCO₃ particles on their uptake by cells. *J Nanobiotechnology.* 2015;13(1):53. doi: 10.1186/s12951-015-0111-7, PMID 26337452.
35. Maver U, Velnar T, Gaberscek M, Planinsek O, Finsgar M. Recent progressive use of atomic force microscopy in biomedical applications. *TrAC Trends Anal Chem.* 2016;80:96-111. doi: 10.1016/j.trac.2016.03.014.
36. Lamprecht C, Hinterdorfer P, Ebner A. Applications of biosensing atomic force microscopy in monitoring drug and nanoparticle delivery. *Expert Opin Drug Deliv.* 2014 Aug 1;11(8):1237-53. doi: 10.1517/17425247.2014.917078, PMID 24809228.
37. Yurtsever A, Wang PX, Priante F, Morais Jaques Y, Miyazawa K, MacLachlan MJ. Molecular insights on the crystalline cellulose-water interfaces via three-dimensional atomic force microscopy. *Sci Adv.* 2022 Oct 14;8(41):eabq0160. doi: 10.1126/sciadv.abq0160, PMID 36240279.
38. Morris VJ, Mackie AR, Wilde PJ, Kirby AR, Mills ECN, Patrick Gunning A. Atomic force microscopy as a tool for interpreting the rheology of food biopolymers at the molecular level. *LWT Food Sci Technol.* 2001 Feb;34(1):3-10. doi: 10.1006/fstl.2000.0706.
39. Joshi J, Homburg SV, Ehrmann A. Atomic force microscopy (AFM) on biopolymers and hydrogels for biotechnological applications-possibilities and limits. *Polymers (Basel).* 2022 Mar 21;14(6):1267. doi: 10.3390/polym14061267, PMID 35335597.
40. Negrea A, Gabor A, Davidescu CM, Ciopec M, Negrea P, Duteanu N. Rare earth elements removal from water using natural polymers. *Sci Rep.* 2018;8(1):316. doi: 10.1038/s41598-017-18623-0, PMID 29321487.
41. Alqaheem Y, Alomair AA. Microscopy and spectroscopy techniques for characterization of polymeric membranes. *Membranes (Basel).* 2020 Feb 24;10(2):33. doi: 10.3390/membranes10020033, PMID 32102383.
42. Brown RJ, Tsuzuki T, Rainey TJ. A comparison of cellulose nanocrystals and cellulose nanofibres extracted from bagasse using acid and ball milling methods. *Adv Nat Sci Nanosci Nanotechnol.* 2016 Sep 1;7(3).
43. Daicho K, Saito T, Fujisawa S, Isogai A. The crystallinity of nanocellulose: dispersion-induced disordering of the grain boundary in biologically structured cellulose. *ACS Appl Nano Mater.* 2018 Oct 26;1(10):5774-85. doi: 10.1021/acsanm.8b01438.
44. Tanpichai S, Biswas SK, Witayakran S, Yano H. Water hyacinth: A sustainable lignin-poor cellulose source for the production of cellulose nanofibers. *ACS Sustainable Chem Eng.* 2019 Dec 2;7(23):18884-93. doi: 10.1021/acssuschemeng.9b04095.
45. Nikonenko NA, Buslov DK, Sushko NI, Zhibankov RG. Investigation of stretching vibrations of glycosidic linkages in disaccharides and polysaccharides with use of IR spectra deconvolution. *Biopolymers.* 2000 Jan 1;57(4):257-62. doi: 10.1002/1097-0282(2000)57:4<257::AID-BIP7>3.0.CO;2-3.
46. Rahimi M, Brown R, Tsuzuki T, Rainey T. A comparison of cellulose nanocrystals and cellulose nanofibres extracted from bagasse using acid and ball milling methods. *Adv Nat Sci Nanosci Nanotechnol.* 2016 Jul 5;7:035004.
47. Chieng B, Lee S, Ibrahim N, Then Y, Loo Y. Isolation and characterization of cellulose nanocrystals from oil palm mesocarp. *Fibers Polym (Basel).* 2017 Aug 11;9(12):355.
48. Radakisnin R, Abdul Majid MS, Jamir MRM, Jawaid M, Sultan MTH, Mat Tahir MF. Structural, morphological and thermal properties of cellulose nanofibers from napier fiber (*Pennisetum purpureum*). *Materials (Basel).* 2020 Sep 1;13(18). doi: 10.3390/ma13184125, PMID 32957438.
49. Maiti S, Jayaramudu J, Das K, Reddy SM, Sadiku R, Ray SS. Preparation and characterization of nano-cellulose with new shape from different precursor. *Carbohydr Polym.* 2013;98(1):562-7. doi: 10.1016/j.carbpol.2013.06.029, PMID 23987382.
50. Patil TV, Patel DK, Dutta SD, Ganguly K, Santra TS, Lim KT. Nanocellulose, a versatile platform: From the delivery of active molecules to tissue engineering applications. *Bioact Mater.* 2022;9:566-89. doi: 10.1016/j.bioactmat.2021.07.006, PMID 34820589.
51. Peltonen L. Practical guidelines for the characterization and quality control of pure drug nanoparticles and nano-cocrystals in the pharmaceutical industry. *Adv Drug Deliv Rev.* 2018;131:101-15. doi: 10.1016/j.addr.2018.06.009, PMID 29920294.
52. Lin SY, Wang SL. Advances in simultaneous DSC-FTIR microspectroscopy for rapid solid-state chemical stability studies: some dipeptide drugs as examples. *Adv Drug Deliv Rev.* 2012;64(5):461-78. doi: 10.1016/j.addr.2012.01.009, PMID 22300653.
53. Antlauf M, Boulanger N, Berglund L, Oksman K, Andersson O. Thermal conductivity of cellulose fibers in different size scales and densities. *Biomacromolecules.* 2021 Sep 13;22(9):3800-9. doi: 10.1021/acs.biomac.1c00643. PMID 34510907.